Solar prominence diagnostics from non-LTE modelling of Mg II h&k line profiles

A.W. Peat[1], N. Labrosse[1], B. Schmieder[1, 2, 3], K. Barczynski[2, 4, 5]

[1]SUPA School of Physics and Astronomy, The University of Glasgow, UK
[2]LESIA, Observatoire de Paris, Université PSL, France
[3]KU Leuven, Belgium
[4]PMOD/WRC, Switzerland
[5]ETH-Zurich, Zürich, Switzerland

We investigate a new method to for obtaining the plasma parameters of solar prominences observed in the Mg II h&k spectrallines by comparing line profiles from the IRIS satellite to a bank of profiles computed with a one-dimensional non-local thermody-namic equilibrium (non-LTE) radiative transfer code.

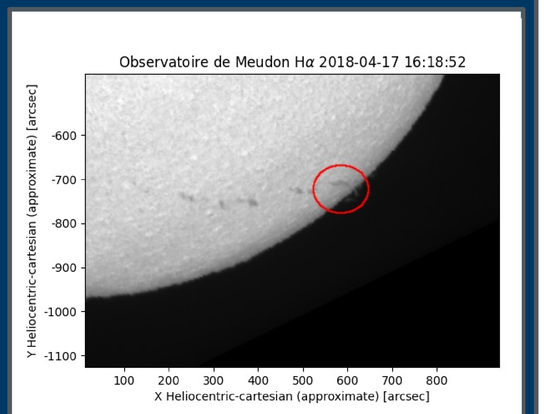

A filament appeared on the south-western solar disc on 17 April 2018 in Hα observations from the Meudon Spectroheliograph. This later manifested as a prominence off the south-western solar limb on 19 April 2018. The prominence was observed with IRIS, and Hinode as part of a coordinated observation with MSDP and other ground-based observatories. The IRIS and Hinode observations start from 14:14 and end at 19:15 UTC. The IRIS observations comprise of a set of 18 very large coarse 32-step rasters of the C II (1331.7 Å to 1358.3 Å), Si IV (1388.0Åto 1406.7 Å), and Mg II (2783.2 Å to 2835 Å) filters, with their complimentary SJI observations centred at 1330 Å, 1400 Å, and 2796 Å. The rasters had a field of view (FOV) of 63.9″×182.3″ centred on helioprojective coordinates 632.5″, -753.2″, with a clockwise satellite rotation angle of 51°. The Hinode observations consisted of XRT observations with three filter combinations, Al poly/Open, Open/Gband, and Open/Ti with an FOV of 263.3″×263.3″, centred on helioprojective coordinates 607.2″, -749.7″. The MSDP observations start at 12:05 UTC and end at 16:35 UTC with a reconstructed FOV of 270″×370″.

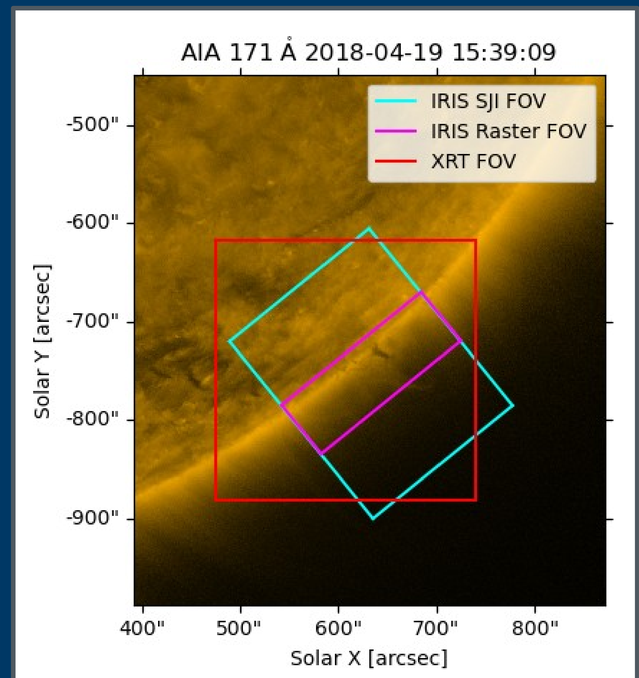

SDO/AIA 171 Å clearly shows a pillar-like barb of the prominence extending in to the fainter main body and/or PCTR.

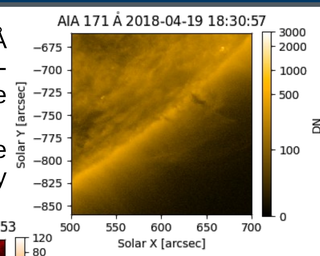

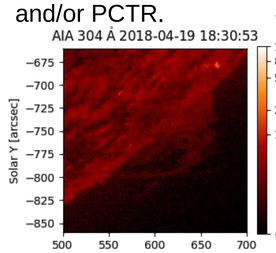

SDO/AIA 304 Å gives a more dynamic view of the cooler and denser material of the prominence.

IRIS/SJI 2796 Å shows similar morphology and evolution than 304 Å, however the limb appears much lower.

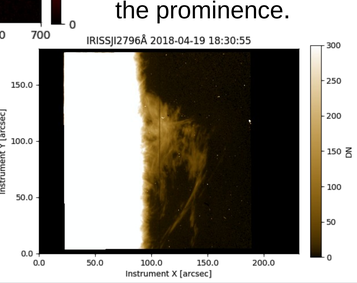

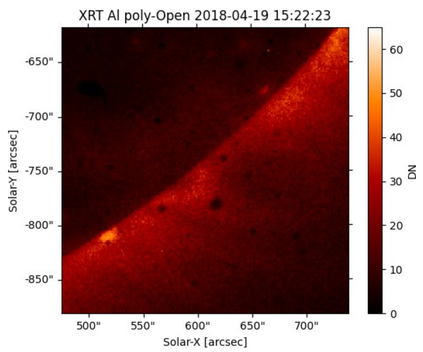

The images from the Al poly/Open filter of XRT on board Hinode clearly show the coronal cavity in which the prominence sits. However, over the course of the observation, these images do not show any appreciable change or brightenings

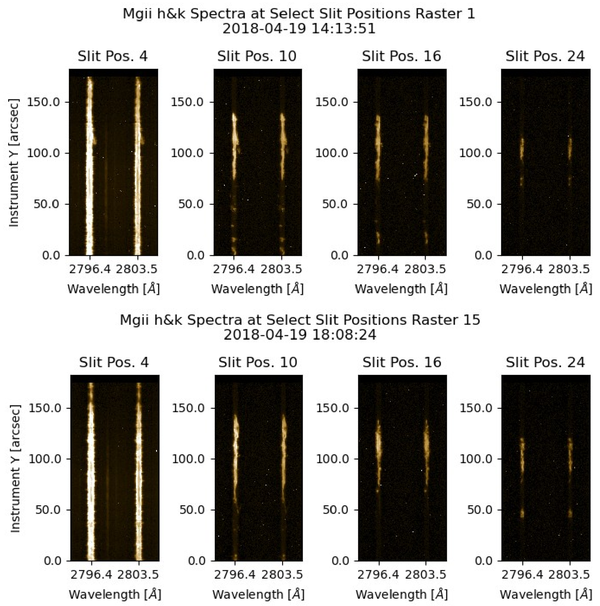

Some of the Mg II h&k spectra obtained by IRIS show complex structure. This implies that some regions of the prominence havemore than one structure along the line of sight. A notable example is seen in the left figure near 120″ in slit position 7. Here we see what appears to be a single peaked profile in Mg II h&k with a secondary redshifted peak. This is not unique to this slit position, however, it is the most extreme case.

The prominence presents a variety of line profile types. These were found by using a finite difference approximation of the derivative of values above the standard deviation of the intensity of the currently considered pixel. From this, stationary points could be counted. If two, or more than three stationary points were found, the line profile was classified as complex.

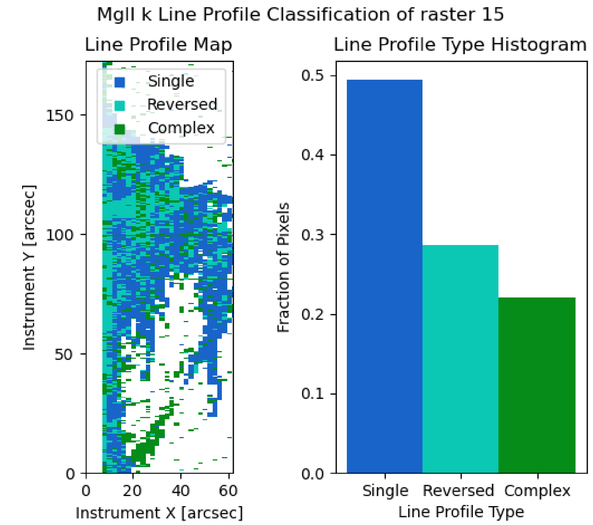

Solar prominence diagnostics from non-LTE modelling of MgII h&k line profiles

A.W. Peat[1], N. Labrosse[1], B. Schmieder[1, 2, 3], K. Barczynski[2, 4, 5]

[1]SUPA School of Physics and Astronomy, The University of Glasgow, UK
[2]LESIA, Observatoire de Paris, Université PSL, France
[3]KU Leuven, Belgium
[4]PMOD/WRC, Switzerland
[5]ETH-Zurich, Zürich, Switzerland

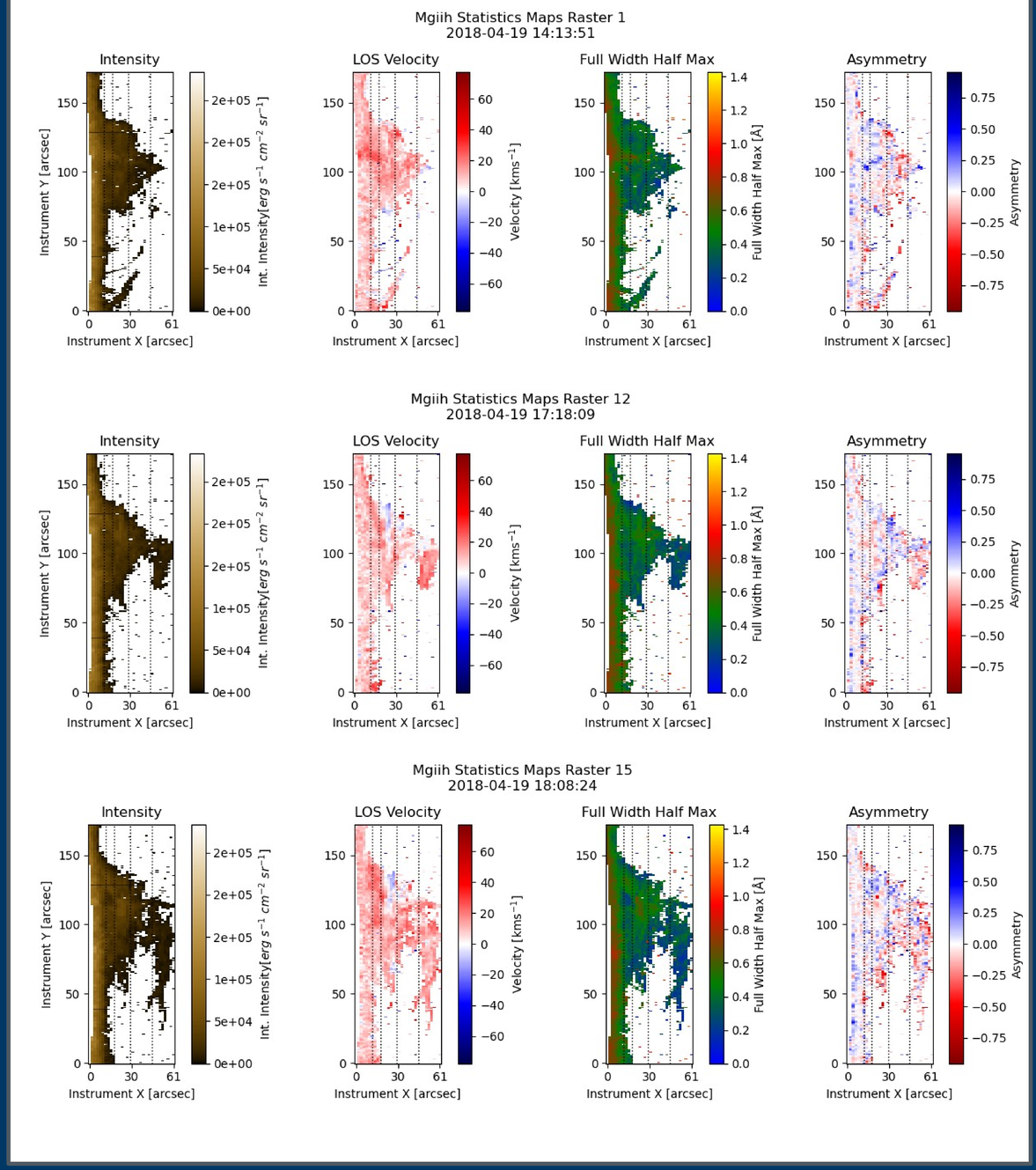

$$\frac{\int_{\lambda_0}^{\lambda_{12}} I(\lambda)d\lambda}{\int_{\lambda_0}^{\lambda_1} I(\lambda)d\lambda} = 0.12 \qquad \frac{\int_{\lambda_0}^{\lambda_{50}} I(\lambda)d\lambda}{\int_{\lambda_0}^{\lambda_1} I(\lambda)d\lambda} = 0.50$$

$$\frac{\int_{\lambda_0}^{\lambda_{88}} I(\lambda)d\lambda}{\int_{\lambda_0}^{\lambda_1} I(\lambda)d\lambda} = 0.88$$

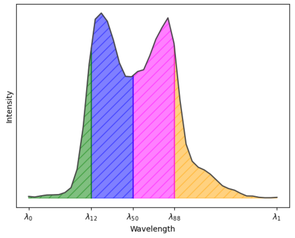

$$\mathrm{FWHM} = \lambda_{88} - \lambda_{12} \qquad v = c\left(\frac{\lambda_e}{\lambda_{50}} - 1\right)$$

$$\mathrm{Asymmetry} = \frac{(\lambda_{88} - \lambda_{50}) - (\lambda_{50} - \lambda_{12})}{\lambda_{88} - \lambda_{12}}$$

Here we use the quantile method to determine the FWHM, line core shift, and asymmetry of the line profiles to investigate the internal structure and dynamics of the prominence.
The quantile method involves calculating the cumulative distribution function (CDF) of the intensity of the individual line profiles over some wavelength range. Here, we employ a 3Å window centred on the rest vacuum wavelengths of MgII h&k. The wavelength at which the 50% level of the CDF is found (λ50) is defined as the line core. Including the 12% and 88% level (λ12 and λ88) we can calculate the aforementioned quantities.

The total velocity distributions are a Gaussian-like centred on a redshifted line core of around 8.20kms^{-1} and 5.20kms^{-1} with standard deviations of 5 .98kms^{-1} and 6.61kms^{-1} in MgII h&k, respectively.

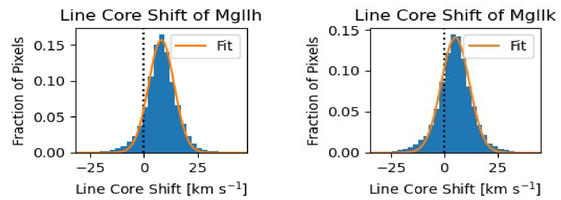

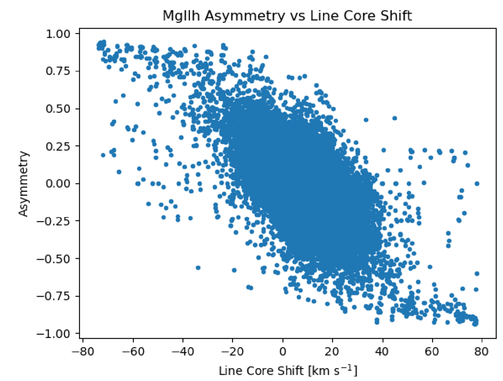

The wings of the Gaussian fits used in the above left figure do not seem to model the velocity distributions well. The cause of this shape is suggested by the figure above right. Asymmetry and measured Doppler velocity appear to be anti-correlated, plateauing at high measured velocities.
The root of this trend lies in the optical thickness of the lines. At rest, the line cores of MgII h&k are optically thick, but the wings are optically thin. Therefore, line profiles of high redshift will display a negative (red) asymmetry due to h_{2v} and k_{2v} being shifted into the more optically thick area of the line. This leads to the quantile method measuring a larger-than-true velocity due to the absorbed h_{2v} and k_{2v} giving more credence to the intensity of h_{2r} and k_{2r}. This effect is amplified by h_{2r} and k_{2r} moving more into the optically thin regime of the wings. The opposite is also true.
The velocities of areas where the asymmetry is much greater than zero are likely unreliable, and only those where the asymmetry is approximately 0, can be considered reliable.

Solar prominence diagnostics from non-LTE modelling of Mg II h&k line profiles

A.W. Peat[1], N. Labrosse[1], B. Schmieder[1, 2, 3], K. Barczynski[2, 4, 5]

[1]SUPA School of Physics and Astronomy, The University of Glasgow, UK
[2]LESIA, Observatoire de Paris, Université PSL, France
[3]KU Leuven, Belgium
[4]PMOD/WRC, Switzerland
[5]ETH-Zurich, Zürich, Switzerland

Using a one-dimensional non local thermal equilibrium radiative transfer code, PROM, we generated 1007 MgII model profiles, 252 of which are isothermal and isobaric, where the remaining 755 include a PCTR The parameters of these atmospheres can be seen right table. All of these combinations amount to 1008 models; however, one model did not converge, so we only consider the 1007 that did.

The PCTR models used here adopt the same parametric description of the PCTR as in Anzer and Heinzel (1999). The pressure profile is given as a function of the column mass m, by

$$p(m) = 4p_c \frac{m}{M}\left(1 - \frac{m}{M}\right) + p_{\rm tr} \qquad \text{where,} \qquad p_{\rm cen} = p_c + p_{\rm tr}$$

The temperature profile is taken to be,

$$T(m) = T_{\rm cen} + (T_{\rm tr} - T_{\rm cen})\left(1 - 4\frac{m}{M}\left(1 - \frac{m}{M}\right)\right)^{\gamma}$$

γ is a dimensionless number that dictates the extent of the PCTR. A γ value of 0 indicates the model is isothermal and isobaric – with no PCTR. γ, however, cannot physically be zero, it is a placeholder.

Parameter	Unit	Value
$T_{\rm cen}$	K	6000, 8000, 10000, 15000, 20000, 25000, 30000, 35000, 40000
$T_{\rm tr}$	K	100000
$p_{\rm cen}$	dyne cm^{-2}	0.01, 0.02, 0.05, 0.1, 0.2, 0.5, 1
$p_{\rm tr}$	dyne cm^{-2}	0.01
Slab Width	km	200 – 124100
M	g cm^{-2}	3.7×10^{-8}–5.1×10^{-4}
v_T	km s^{-1}	5
H	km	1000
γ		0, 2, 5, 10

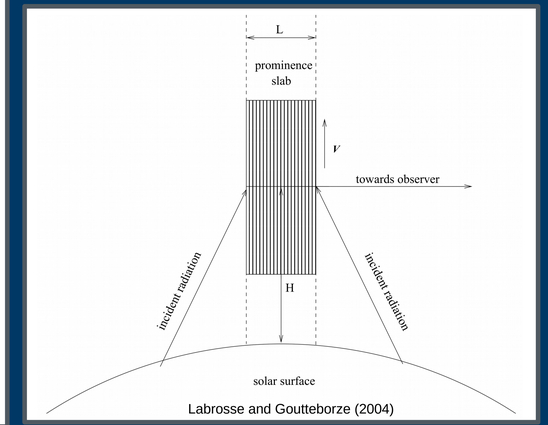

Labrosse and Goutteborze (2004)

To match these line profiles directly with IRIS observations, we must first degrade the line profiles to match the spectral resolution of IRIS.

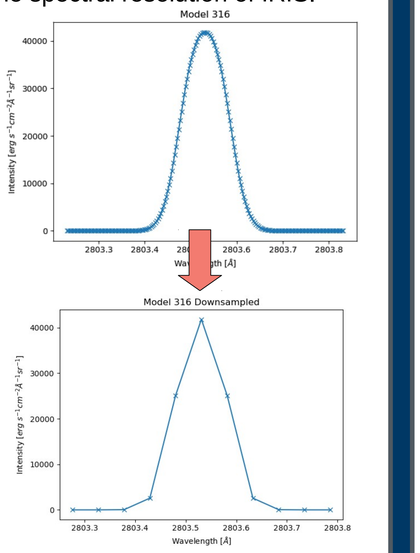

We also employ sub-pixel interpolation to allow us to get better matches. We do this as the peaks of many profiles appear to exist somwhere between “two pixels” and we wish to allow the peaks to line up as well as possible.

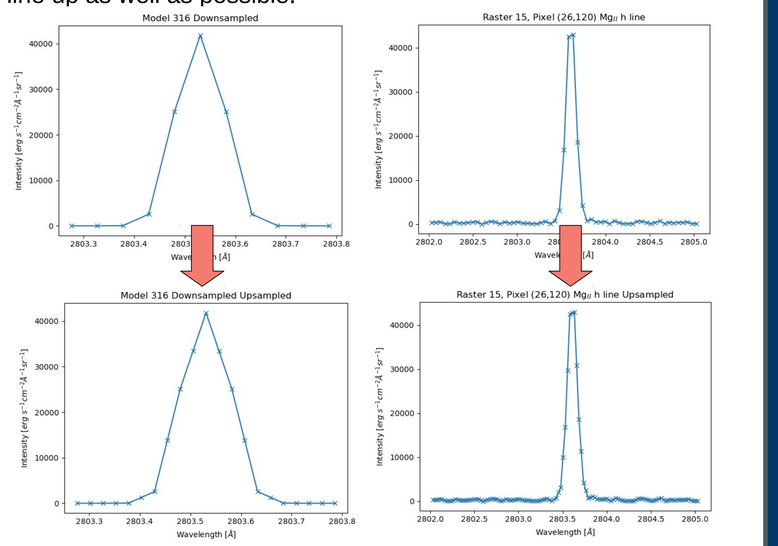

We wish to match these synthesized line profiles with observations. However, these synthesized profiles are formed at exactly the rest wavelength of the line(s). This is rarely (if at all) seen in reality. To account for this, we “roll” the synthesized line profiles through some window (here, 3Å) centred on the rest wavelength of the lines, measuring the RMS at every position.

This allows us to find the “best fitting” line, independent of doppler velocity. As we measure RMS, we also have a statistic to determine how well a synthesized profile fits the observations.

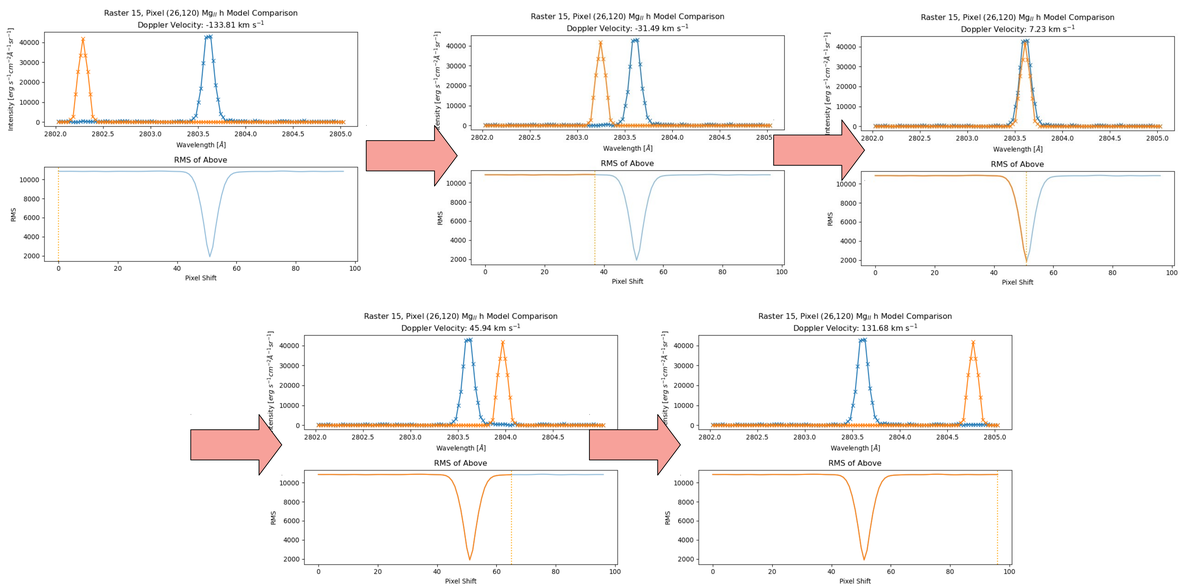

This Rolling RMS method (rRMS) recovers the following best fit position for model 316 in one of the IRIS pixels. A corollary of this procedure is that we are able to recover the doppler velocity for this pixel. If we know how many spectral pixels the synthesized profile was shifted to achieve a best fit, we can use this to measure doppler velocity. Doppler maps can then be compared against doppler maps from the quantile method to test the efficacy of this method

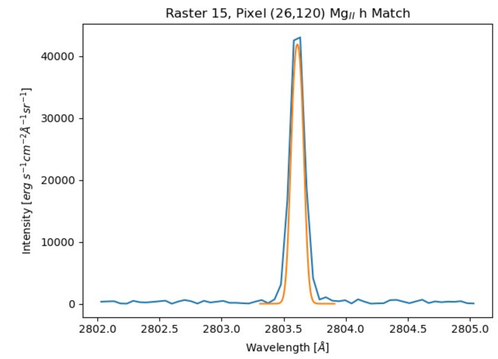

Solar prominence diagnostics from non-LTE modelling of Mg II h&k line profiles

A.W. Peat[1], N. Labrosse[1], B. Schmieder[1, 2, 3], K. Barczynski[2, 4, 5]

[1]SUPA School of Physics and Astronomy, The University of Glasgow, UK
[2]LESIA, Observatoire de Paris, Université PSL, France
[3]KU Leuven, Belgium
[4]PMOD/WRC, Switzerland
[5]ETH-Zurich, Zürich, Switzerland

rRMS is run on every pixel of every raster for all 1007 models.
A cut off value for a good vs bad match was determined manually by checking a set of 12 matches where 6 were determined to be unsatisfactory and 6 were determined to be satisfactory. From this, a cut of value was found. Allowing us to confidentally assert the conditions of the prominence.

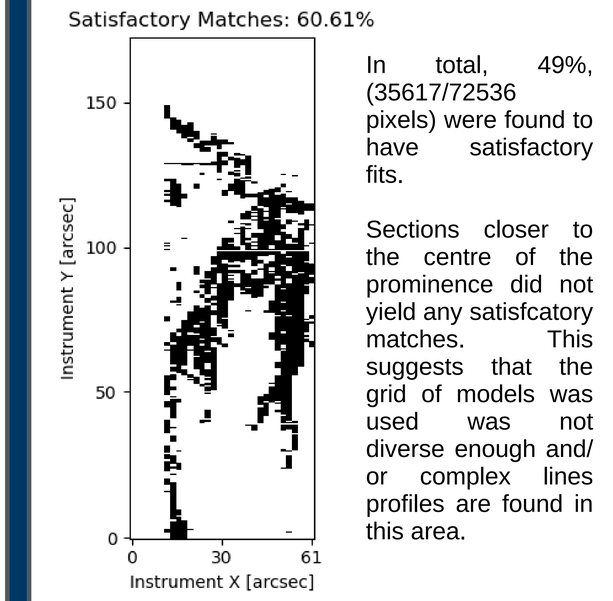

In total, 49%, (35617/72536 pixels) were found to have satisfactory fits.

Sections closer to the centre of the prominence did not yield any satisfcatory matches. This suggests that the grid of models was used was not diverse enough and/ or complex lines profiles are found in this area.

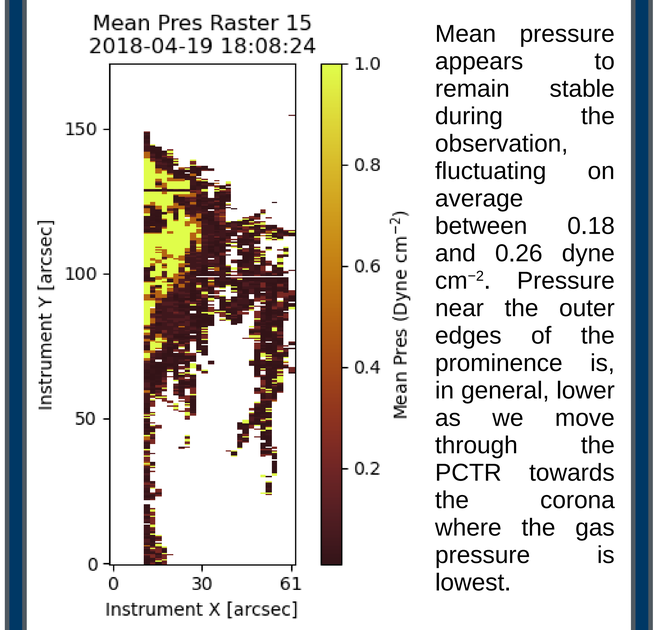

Mean pressure appears to remain stable during the observation, fluctuating on average between 0.18 and 0.26 dyne cm^{-2}. Pressure near the outer edges of the prominence is, in general, lower as we move through the PCTR towards the corona where the gas pressure is lowest.

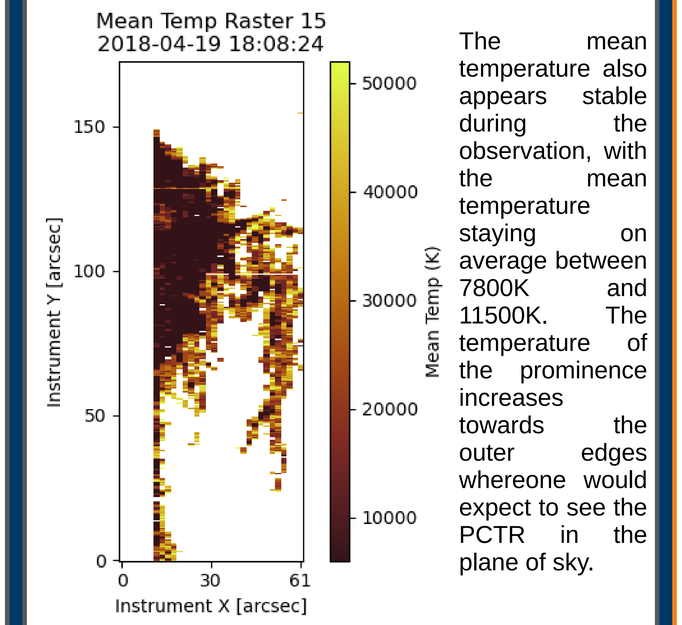

The mean temperature also appears stable during the observation, with the mean temperature staying on average between 7800K and 11500K. The temperature of the prominence increases towards the outer edges whereone would expect to see the PCTR in the plane of sky.

To conclude, we recover satisfactory diagnostics of the prominence.
Satisifactory matches were failed to be found in areas closer to the centre of the prominence.
In future, a more diverse grid of models could be employed to achieve better matches with that of the observations.
Another route would be to utilise multithread model to attempt to account for complex line profiles.

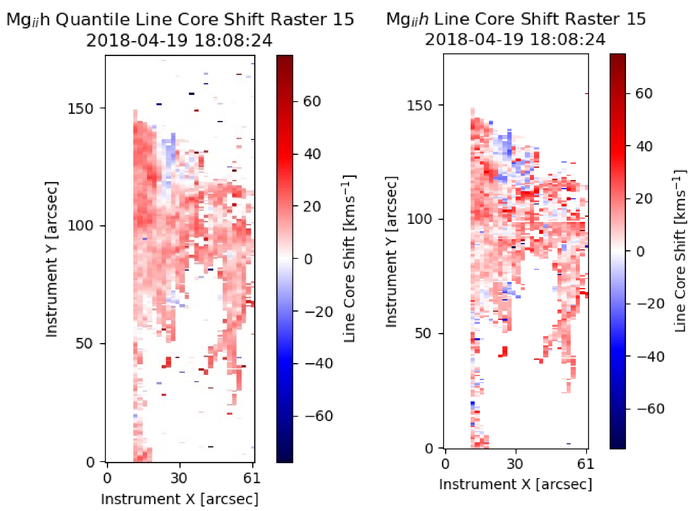

As asymmerty bias affects the line core shift measured by the quantile method, we present only a qualitative match between the line core shift from rRMS and the quantile method. Generally, these maps appear consistent with one another, showing that the “rolling” aspect of the procedure is working as intended.

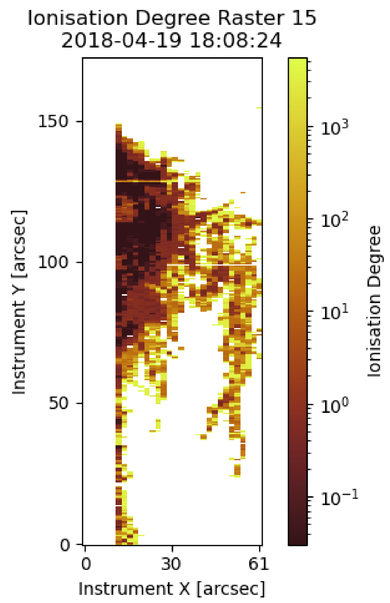

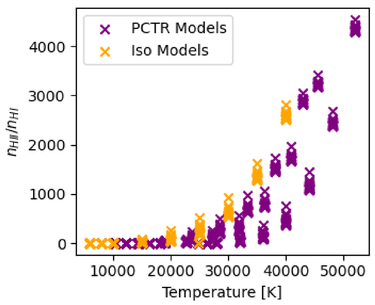

Past studies show that the ionisation degree (nHII/nHI) is within 0 to 10. However, these past studies never considered temperatures above 15000K. Above these temperatures, the ionisation degree increases exponentially. The higher temperatures that we recover lead to a higher ionisation degree.

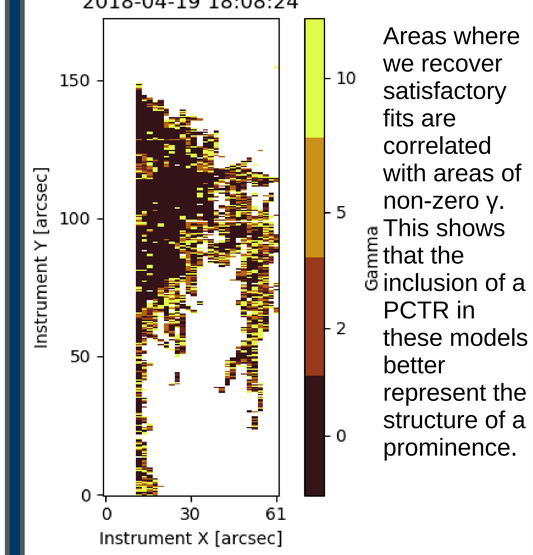

Areas where we recover satisfactory fits are correlated with areas of non-zero γ. This shows that the inclusion of a PCTR in these models better represent the structure of a prominence.